Chemistry—Methods

Research Article
doi.org/10.1002/cmtd.202200008

Chemistry Europe
European Chemical Societies Publishing

www.chemistrymethods.org

Data-Driven Analysis of High-Throughput Experiments on Liquid Battery Electrolyte Formulations: Unraveling the Impact of Composition on Conductivity**

Anand Narayanan Krishnamoorthy,[a] Christian Wölke,[a] Diddo Diddens,[a] Moumita Maiti,[c] Youssef Mabrouk,[a] Peng Yan,[a] Mariano Grünebaum,[a] Martin Winter,[a, b] Andreas Heuer,*[a, c] and Isidora Cekic-Laskovic*[a]

A specially designed high-throughput experimentation facility, used for the highly effective exploration of electrolyte formulations in composition space for diverse battery chemistries and targeted applications, is presented. It follows a high-throughput formulation-characterization-optimization chain based on a set of previously established electrolyte-related requirements. Here, the facility is used to acquire large dataset of ionic conductivities of non-aqueous battery electrolytes in the conducting salt-solvent/co-solvent-additive composition space. The measured temperature dependence is mapped on three generalized Arrhenius parameters, including deviations from simple activated dynamics. This reduced dataset is thereafter analyzed by a scalable data-driven workflow, based on linear and Gaussian process regression, providing detailed information about the compositional dependence of the conductivity. Complete insensitivity to the addition of electrolyte additives for otherwise constant molar composition is observed. Quantitative dependencies, for example, on the temperature-dependent conducting salt content for optimum conductivity are provided and discussed in light of physical properties such as viscosity and ion association effects.

Introduction

High-throughput (HT) strategies allow researchers to perform multiple experiments within a relatively short time in parallel to accelerate material discovery process.[1,2] Such strategies are generally achieved by using rapid automation tools including a large combination of material variables.[3] These methods are predominantly used in biological and pharmaceutical industries.[4–7] Further HT methods are nowadays used in other industries beyond pharma.[8–11] Recent efforts have been made to use HT methods to discover and optimize materials for battery cell chemistries.[12,13] High-throughput experimentation (HTE) systems represent a highly valuable tool for accelerating the search towards advanced and optimized battery materials and with it, electrolyte formulations for given cell chemistry candidates, electrode-electrolyte interfaces, overall cell performance, safety and cost. Recently, computational screening methodologies have been used to effectively support the battery material discovery process and a combinatorial approach of experiments and computational approach has been discussed as a way forward in the battery material discovery process.[14,15] Data driven models are predominantly used to extract knowledge and insights from noisy, structured and unstructured datasets.[16–19] Optimization of datasets (features, number of samples) are required to increase the efficiency of such models.[20–23] Currently artificial intelligence (AI) and machine learning algorithms are transforming material discovery processes, especially in battery science.[24,25]

The performance of all batteries (including Li-ion analogues) is governed by the nature of electrolytes used. The ionic conductivity in a liquid electrolyte, for instance, co-determines the rate of the charging process. Organic solvent-based electrolyte formulations are of central relevance and still considered as state-of-the-art.[26,27] Common electrolyte formulations consist of lithium conducting salt such as lithium hexafluorophosphate ($LiPF_6$) and solvent mixtures comprising cyclic carbonates like ethylene carbonate (EC) and propylene carbonate (PC) with linear organic carbonates like dimethyl carbonate (DMC), ethyl methyl carbonate (EMC) and diethyl carbonate (DEC) and

[a] Dr. A. Narayanan Krishnamoorthy, Dr. C. Wölke, Dr. D. Diddens, Y. Mabrouk, P. Yan, Dr. M. Grünebaum, Prof. Dr. M. Winter, Prof. Dr. A. Heuer, Dr. I. Cekic-Laskovic
Helmholtz-Institute Münster (IEK-12)
Forschungszentrum Jülich GmbH
Corrensstraße 46
48149 Münster (Germany)
E-mail: andheuer@uni-muenster.de
i.cekic-laskovic@fz-juelich.de

[b] Prof. Dr. M. Winter
MEET Battery Research Center
University of Münster
Corrensstrasse 46
48149 Münster (Germany)

[c] Dr. M. Maiti, Prof. Dr. A. Heuer
Institute of Physical Chemistry
University of Münster
Corrensstrasse 28/30
48149 Münster (Germany)

[**] A previous version of this manuscript has been deposited on a preprint server (https://doi.org/10.26434/chemrxiv-2022-vbl5d)

Supporting information for this article is available on the WWW under https://doi.org/10.1002/cmtd.202200008

Research Article
doi.org/10.1002/cmtd.202200008
Chemistry Europe
European Chemical Societies Publishing

provide desirable electrochemical properties for Li-ion batteries.[28–33]

Results and Discussion

Here we perform HT impedance spectroscopic experiments on $LiPF_6$-based electrolyte formulations containing EC and EMC as solvent mixture and vinylene carbonate (VC) as functional additive/co-solvent to determine ionic conductivities of resulting electrolyte formulations and develop a data driven model to predict ionic conductivities for variable electrolyte compositions. The established conductivity module is quite flexible in nature and can be extended to other liquid-based electrolyte classes including sodium, potassium, magnesium, calcium chemistries with wide variety of conducting salts, solvents/co-solvents and functional additives. All data are extracted from HT experiments with conducting salt, solvent/co-solvent, additive compositions and temperature as features and ionic conductivity as target quantity. The electrolyte module of the HTE system, developed in-house, is composed of two independent, however well-connected units under a N_2 atmosphere (Figure 1A). In regard to the electrolyte formulation, all considered electrolyte components have to be manually introduced to the HTS System I through the bridging chamber in which the corresponding containers are being filled up with electrolyte components. From this point, the system, governed by Laboratory Information Management System (LIMS), formulates electrolytes and consequently fills conductivity cells with corresponding electrolyte formulations in a fully automated way. After initial programming and filling of the dosing units with electrolyte components, the HTE unit fully automatically conducts fast and systematic formulation of up to 96 different liquid electrolytes per working day. The system is capable of handling a wide variety of lithium conducting salts, solvents/co-solvents and (multi)-functional additives as electrolyte components in solid and liquid form that can be combined with respect to their presence and amount in a considered electrolyte formulation.

The robotic platform was developed by combining multiple functionalities to an integrated platform system. It is composed

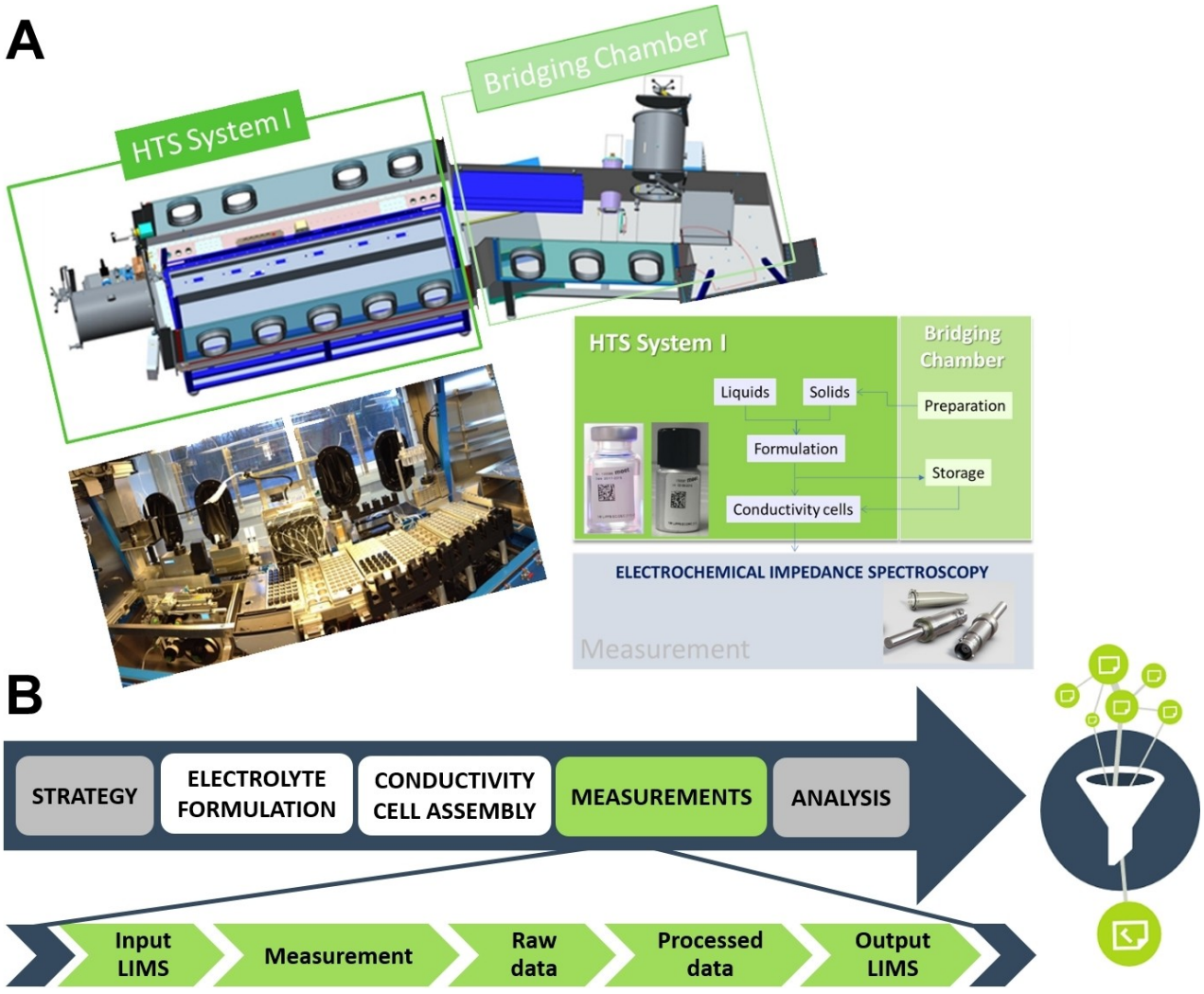

Figure 1. A) Electrolyte module featuring an automated HT system for electrolyte formulation and conductivity cell assembly with bridging chamber used for storage and preparation activities. B) Flow chart of an automated electrolyte formulation to conductivity determination and analysis sequence.

Research Article
doi.org/10.1002/cmtd.202200008
Chemistry Europe
European Chemical Societies Publishing

of 21 stations enabling required gravimetric solid and liquid dispensing of selected electrolyte components with high accuracy (0.026% for solids and 0.024% for liquids), vial closing, vial mixing and heating and vial barcode labeling steps within the electrolyte formulation workflow (Figure 1B). A data matrix barcode contains all relevant information regarding the electrolyte composition and components like their amount, supplier, date of formulation and is easily readable by a smartphone app. The end-product is a cyclic olefin polymer vial, crimped with electrolyte resistant needle piercing septum or a screw cap aluminum vial and contains a maximum 10 mL of electrolyte formulation. Within the HTE unit, an automated filling of conductivity cells with electrolyte is performed after optional visual examination of the electrolytes as well. The second unit of the electrolyte module is the bridging chamber, fused for preparation and storage purposes, positioned in the glovebox under N_2 atmosphere.

For the electrolyte conductivity determination by means of electrochemical impedance spectroscopy (EIS), a conductivity module consisting of 96 measuring cells was developed. Considered electrolyte formulations were dispensed into disposable Eppendorf Safe-Lock Tubes in small sample quantities (750 µL) by the HTE robotic system in the glovebox under N_2 atmosphere. In-house developed electrodes were thereafter immersed in the electrolytes (Figure 2A(a)). These electrodes as measuring probes deliver reproducible results regardless of the immersion depth in the electrolyte or the sample container geometry in the impedance measurements.[34] Eight conductivity cells were placed on a small rack (Figure 2A(b)) and three of the small racks were positioned on a big rack (Figure 2A(c)) for a total of 24 conductivity cells per big rack. Four big racks resulted in a total of 96 conductivity cells. To obtain the data on the internal resistance and conductivity of the electrolyte formulations, a Metrohm Autolab potentiostat/galvanostat with 8×12-channel multiplexer was used. The multiplexer, based on a particularly powerful single-board micro-controller, is capable of multiplexing each of the 12 potentiostat/galvanostat channels 8-fold, thus resulting in 96 controllable channels (Figure 2A(d)). The assembled conductivity cells have to be manually taken out of the HTS System I and placed in the climate chamber with a 2-hour equilibration period for any given temperature prior to each measurement. Measurements were conducted in the temperature range from 0 °C to 60 °C in 10 °C increments. Once the potentiostat is connected to the

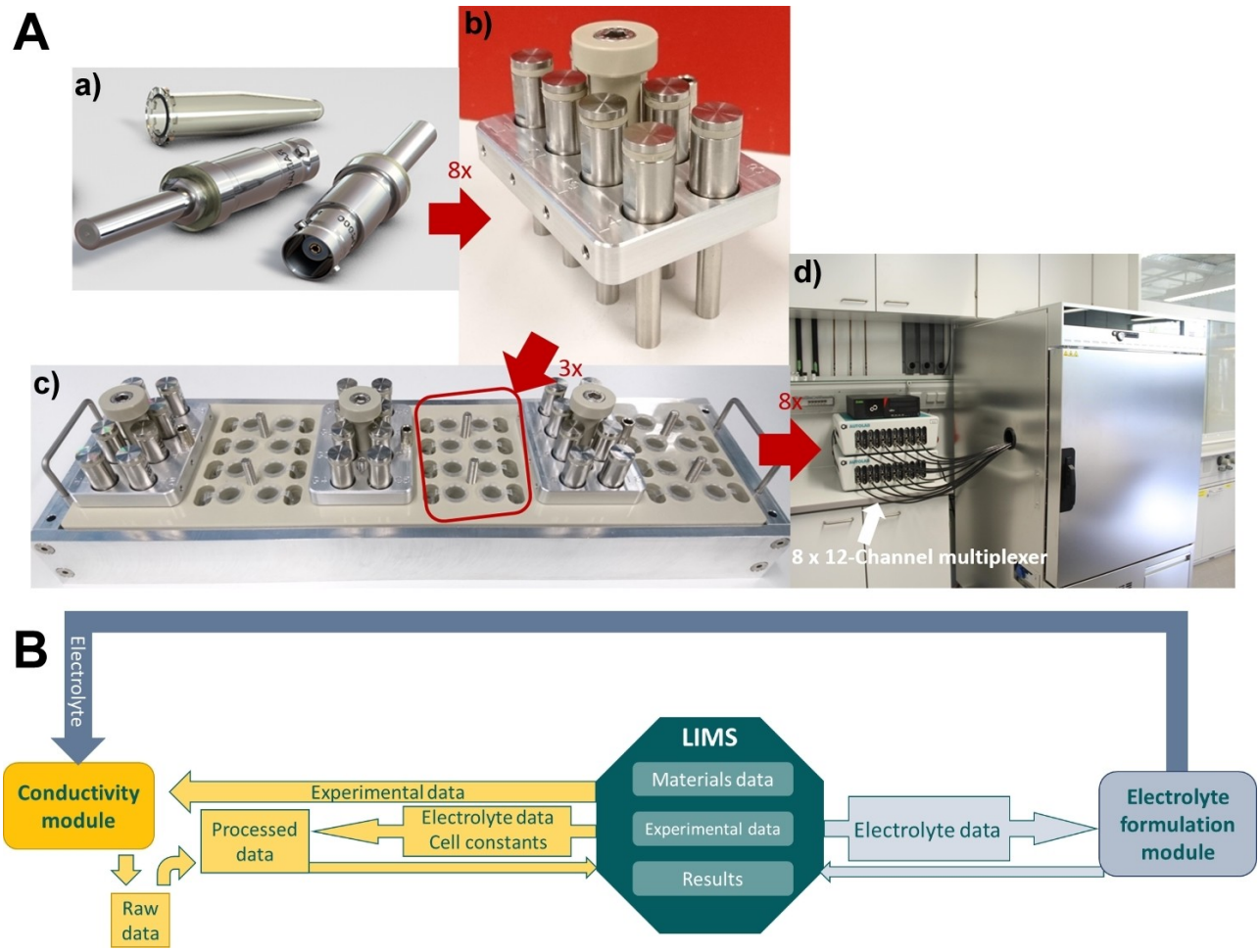

Figure 2. A) Conductivity module comprising: a) in-house developed coaxial impedance electrode and Eppendorf tube b) small rack containing 8 electrodes c) big rack with 24 conductivity cells and d) potentiostat/galvanostat with 8×12-channel multiplexer and temperature chamber. B) Schematic overview of the LIMS-modules interaction workflow.

conductivity cells and programmed with a temperature sequence by the operator, the setup requires no further user input.

Both electrolyte formulation and conductivity modules of the HTE facility are operated independently by a customized instance of the LIMS adjusted to the specific system by the Quality Systems International (QSI) GmbH. The value chain, governed by the LIMS, is depicted in Figure 2B. As the system's central entity, this software, flexible in nature, also serves as a material and data archive that ensures data provenance and enables backtracking of experiments. Materials data include specific identifiers (supplier, batch number, purity etc.) whereas experimental data consists of test protocols and relevant experimental parameters such as temperature. Besides saving the raw experimental data, the system is capable of processing the raw results and bundling them with relevant metadata (relevant details on the used electrolyte) into a machine-readable output format in order to provide users with all available information on a given experiment.

For the experiments reported in this work, the applied EC to EMC ratios were 3 : 7, 3 : 2 and 3 : 1 by weight with a VC content between 0 and 30 wt% with respect to EC and EMC. At the same time, the concentration of $LiPF_6$ was varied between 0.2 and 2.3 mol/kg. Exact amounts of all components for each electrolyte formulation can be found in the Supporting Information (Table S1 and Table S2). Considering 7 different temperatures and repetition of each measurement for at least 3 times in respect to reproducibility for each electrolyte formulation, the total number of experimentally obtained data points amounted to 1200.

For data analysis, a molar description of the electrolyte via x_{LiPF6} $LiPF_6 \cdot (1\text{-}x_{LiPF6})[x_{VC}$ $VC \cdot (1\text{-}x_{VC})$ $[x_{EC}$ $EC \cdot (1\text{-}x_{EC})$ EMC]] was used. In this representation, the EC/EMC ratio does not change under variation of the VC content, x_{VC}. The ranges were chosen to cover a broad section of the composition space where feasible electrolyte formulations can be expected (i.e., homogeneous solutions). However, in some formulations with high EC and $LiPF_6$ content, crystal formation occurred, rendering these formulations unusable (see Figures S3–S7). NMR analysis revealed that the crystals taken from one of the formulations only consist of $LiPF_6$ and EC, implying that the crystallizing compound is likely $Li(EC)_4PF_6$.[35] Some electrolyte formulations with low $LiPF_6$ and high EC content showed anomalous conductivity values at low temperatures, indicating freezing of EC (see Figure S5).

To provide a deeper understanding of HT datasets, conductivities are transformed according to the generalized Arrhenius fit ($X = (x_{LiPF6}, x_{VC}, x_{EC})$) [Eq. (1)]:

$$\boldsymbol{log}\sigma(X,T) = S_0(X) - S_1(X)^*(\beta - \beta_0) - S_2(X)^*(\beta - \beta_0)^2 \qquad (1)$$

with the inverse onset temperature β_0. The surrogate models for the description of the $S_i(X)$ are formulated in terms of polynomials. The models as well as the choice of the order, also in the context of the available experimental data sets, are discussed in the methods section of Supporting Information. Of particular relevance is the information content of the in-sample and out-of-sample error as a function of the size of the training set (see Supporting Information V). For the analysis we use dimensionless parameters. In particular, we choose $\beta = 1000/T$ where T is expressed in Kelvin [K]. These parameters have a direct interpretation: $exp[S_0(X)]$ corresponds to the conductivity at the onset temperature. The activation energy, evaluated at the onset temperature, is proportional to $S_1(X)$. Finally, $S_2(X)$ reflects possible deviations from pure Arrhenius behavior, showing up as a curvature. This transformation with implicit temperature description reduces the number of datasets and the corresponding parameters to 3 and all of them have a direct physical interpretation, providing additional information as compared to a polynomial fit of ionic conductivity.[36,37]

The choice of the onset temperature is obtained from the correlation of conductivity and activation energy at a given temperature. At low temperatures both quantities are strongly correlated, since high activation energies show very low conductivities at low temperatures and for the present set of electrolyte compositions this correlation diminishes at approximately 40 °C, as shown in Figure S7.

Here we use linear regression (LR) and Gaussian process regression (GPR) models to analyze the acquired HT electrolyte conductivity datasets. GPR directly provides confidence intervals for the predictions, whereas for LR, we use a bootstrapping process to account for uncertainties in predictions.[17,38–42] The features comprise $LiPF_6$, VC, and EC concentrations and the predicted quantity is the logarithm of the ionic conductivity of the resulting electrolyte. Both LR (R^2 score- 0.986) and GPR (R^2 score- 0.987) show similar prediction accuracy for experimental ionic conductivities which to a large extent are determined by the experimental errors (see Supporting Information V.1)

The data driven workflow is independent of the nature of the dataset, thus can provide a leeway for larger dimensions of features like introduction of multiple co-solvent, additives or conducting salt mixtures. This increased dimensionality of electrolyte formulations increases the complexity of empirical models which are generally used to interpret the relevance of electrolyte compositions on ionic conductivity.[36,37,43] Furthermore, data driven models provide robust error estimates of the predicted data, which are not provided by empirical fits.[17,36,37,44] Thus, these surrogate models provide an effective way to interpret acquired HT datasets independent of feature dimensions. Since both LR and GPR show similar results, we use LR to understand feature trends (x_{LiPF6}, x_{VC}, x_{EC}) on ionic conductivity for convenience. The trends with GPR are shown in Figure S13.

The conductivity at onset temperature $S_0(X)$ tends to increase with $LiPF_6$ content with a peak close to ~(0.07–0.09) and then drops for higher $LiPF_6$ content (Figure 3I, left). A significant dependence on the EC content is observed. Starting from the low $LiPF_6$ content, the initial rise in electrolyte conductivity is typically attributed to an increasing number of dissociated ions per unit volume whereas the subsequent reduction of conductivity reflects the increasing viscosity. The presence of maximum conductivity values upon variation of the conducting salt content has been observed for other lithium-based electrolytes as well.[36,37,43–47] In contrast, the activation energy term $S_1(X)$ and the curvature term $S_2(X)$ show a simple

Research Article
doi.org/10.1002/cmtd.202200008
Chemistry Europe
European Chemical Societies Publishing

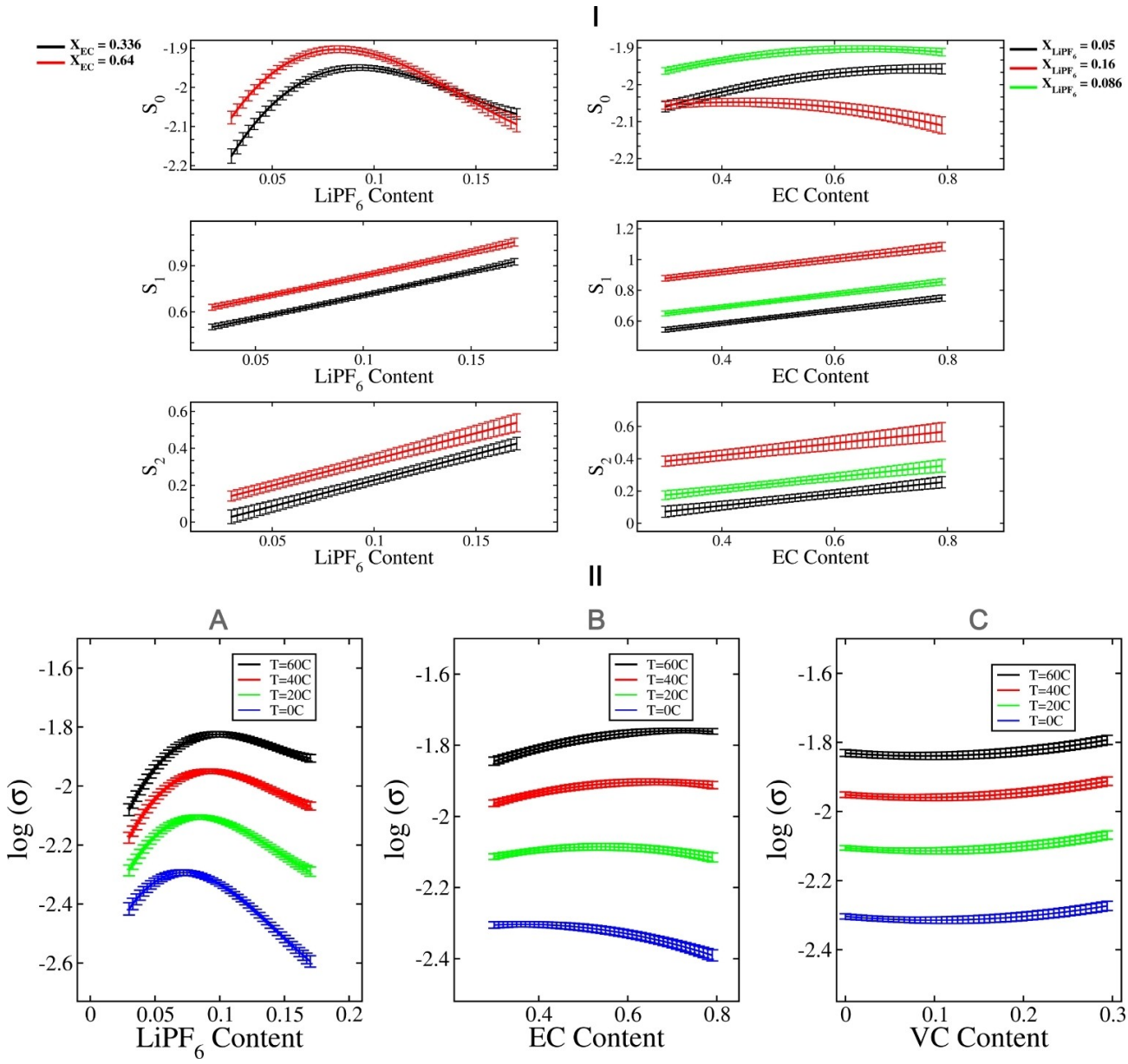

Figure 3. I) Predictions for the generalized Arrhenius fitting parameters $S_i(X)$ (S_0, S_1, S_2) with respect to x_{LiPF6} (left) and x_{EC} content (both for $x_{VC} = 0.0$) (right). II) The change of ionic conductivity with $LiPF_6$ content (A) for fixed [($x_{VC} = 0.0$, $x_{EC} = 0.336$)] EC content (B) for fixed [($x_{VC} = 0.0$, $x_{LiPF6} = 0.086$)] VC content (C) for fixed [($x_{EC} = 0.336$, $x_{LiPF6} = 0.087$)] at different temperatures are shown below. All the results are shown for the LR model.

linear increase with increasing conducting salt content. Higher values are observed for larger EC contents. Further, the resulting influence of temperature on the conductivity is shown in (Figure 3II A). The peak of the conductivity shifts to higher $LiPF_6$ content with increasing temperature.

When analyzing the dependence on EC content, the ionic conductivity at the onset temperature increases with increasing EC content for lower $LiPF_6$ content ($x_{LiPF6} = 0.05$), whereas the trend reverses at higher conducting salt content ($x_{LiPF6} = 0.16$). This directly shows the presence of significant $LiPF_6$ and EC content contributions to the conductivity at the onset temperature which furthermore are coupled (see Supporting Information Table S3). Thus, there is a strong impact of the $LiPF_6$ content on the EC dependent activation energy and curvature (Figure 3I, right). Since the activation energy is just shifted, the impact is not coupled. Also, the dependence on the $LiPF_6$ concentration is more relevant for the transport properties than the replacement of EMC by EC and, for example, the resulting variation of the dielectric constant.[48,49] Consistent with the properties of the activation energy in Figure 3I right, the small peak in conductivity shifts to smaller values of the EC content at lower temperatures.[36]

Finally, the VC content does not play any role in bulk ionic conductivity for fixed EC/EMC ratio as shown in Figure 3II C (see also Table S6). This is a remarkable result, given the similar ring

Research Article
doi.org/10.1002/cmtd.202200008
Chemistry Europe
European Chemical Societies Publishing

structure of EC and VC. However, VC is known to play a pivotal role in electrolyte | electrode interfacial interactions.[50,51]

In Figure 4A, the HTE obtained ionic conductivities, log(σ), for fixed EC/EMC ratio, are compared with other experimental values for the conductivity. The obtained results are compatible within the fluctuations. Furthermore, in Figure 4B we show the logarithm of the molar conductivities and in Figure 4C the activation energies, incorporating data for the viscosity[37,43] and binary diffusivity.[37] Remarkably, the logarithm of the molar conductivities (Figure 4B) as well as the activation energies (Figure 4C) basically display a linear behavior in the whole conducting salt concentration regime. This linear behavior has interesting consequences. As shown in Supporting Information V.6 it allows one to predict the conducting salt content at which the conductivity displays a maximum as a function of temperature, yielding $x_{max}(\beta) = \frac{0.0833}{1+0.76(\beta-\beta_0)}$. The estimations in Figure 4A, based on this relation, indeed show very good agreement with the actual conductivities.

Thus, after removing the trivial impact of an increasing number of ions, there are no indications of changing mechanisms at the maximum. Furthermore, the conducting salt dependence of the molar conductivity at fixed temperature as well as its activation energy is very similar to the respective observables, based on the viscosity. The remaining minor systematic deviations of the activation energies of the conductivity to the viscosity and diffusivity in Figure 4C indicate that the lowering of the conductivity as compared to the Nernst–Einstein prediction via pair formation is somewhat less pronounced for lower temperatures. The latter has been also reported for other systems.[52]

Conclusion

The HT experimentation facility, in general, has the potential to predict a range of vital electrolyte properties and to establish a formulation-characterization-optimization evaluation chain. This involves the discovery of novel and the optimization of existing liquid electrolyte formulations for diverse cell chemistries by using a filtration effect based on the previously established set of requirements for a targeted application. From a first round of preselected, automated experiments,[5,8,9,53–55] lead/hit candidates can be selected and characterized further in subsequent steps. The resulting optimization process may involve the chosen concentrations or the use of different components.

In summary, we propose an in-house developed HT approach to conduct automated impedance experiments in parallel for different electrolyte formulation to attain optimal ionic conductivities. This approach considerably reduces the amount of time required for performing experiments manually and enables accelerated electrolyte discovery process for battery applications. Data driven models, based on 1200 experimentally acquired data points are used to analyze and predict ionic conductivities and can further be utilized to automatically identify outliers and thus increase the robustness of HT experiments. It is shown that considered surrogate models predict ionic conductivities close to experimental accuracies and provide reliable estimates at very low cost compared to actual experiments. The flexibility of the surrogate models with regard to statistical uncertainties provides an effective way to study feature trends on ionic conductivity compared to standard empirical models. The transformed data-driven model provides a physical interpretation of trends of electrolyte compositions on ionic conductivity. Furthermore, additional microscopic simulations and implementation of

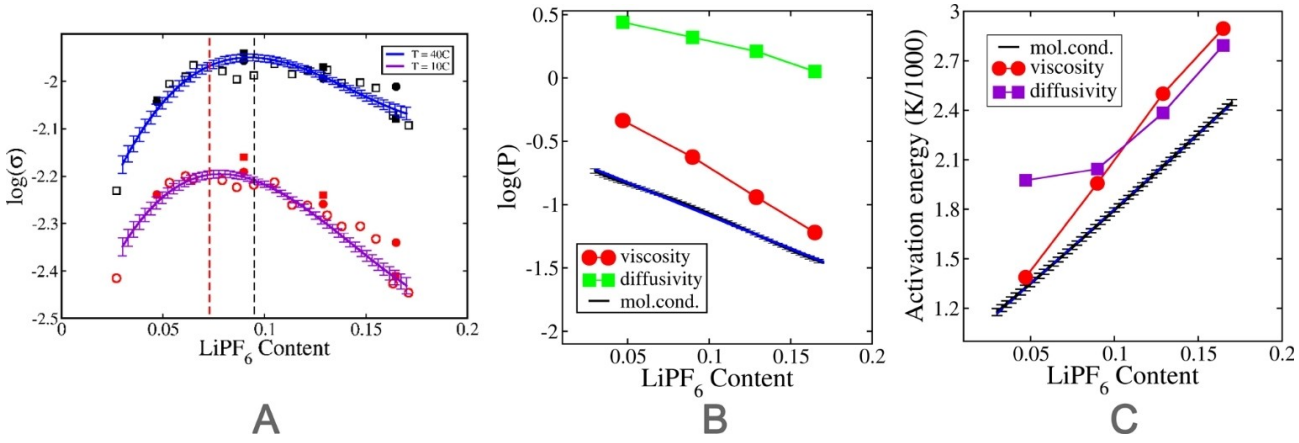

Figure 4. Comparison of different data for the 30:70 wt. EC:EMC system (no VC). (A) The LR conductivity in comparison to the data from Ref. [43] (spheres) and Ref. [37] (squares) at two different temperatures. The broken lines indicate the estimation of the maxima for both temperatures, based on the insight from (B) and (C). For details of the prediction process, see Supporting Information. (B) Comparison of different observables P as a function of conducting salt content at T = 25 °C. Specifically, we show the LR prediction of the logarithm of the molar conductivity σ/x, the negative logarithm of the viscosity [cP] from Ref. [43] (spheres) and the logarithm of diffusivity [10^{-6} cm^2/s] from Ref. [37] (squares). Also included is a linear fit of the logarithm of the molar LR conductivity: −0.56–5.21 x_{LiPF6} (black); as broken line. Due to the excellent agreement with the molar conductivity data, it is hardly visible. (C) Comparison of the activation energies of the LR-based conductivity, the viscosity from Ref. [43] and the diffusivity from Ref. [37] for T = 25 °C. The activation energy of the conductivity has been fitted by 0.89 + 9.1 x_{LiPF6}. The two latter activation energies have been estimated from the viscosity and diffusivity data at T = 40 °C and T = 10 °C from Ref. [43], Ref. [37] respectively. The diffusivity data points at T = 10 °C are estimated from interpolation of data at 12 °C and 2.5 °C as provided in Ref. [37].

closed loop optimization protocols, performed in parallel to the experiments, can increase the efficiency and relative speedup of HTE. This may complement the results from experiments and data driven model, thereby obtaining a holistic understanding of relevant electrolyte formulations. With this in line, important physical and chemical additional insights can be gained.

Experimental Section

Electrolyte formulation

Lithium hexafluorophosphate ($LiPF_6$), ethylene carbonate (EC), ethyl methyl carbonate (EMC) and vinylene carbonate (VC) were purchased from E-Lyte Innovations in battery grade purity. All chemicals were used as received without further purification. Considered electrolytes contain $LiPF_6$ as conducting salt, a mixture of EC and EMC as electrolyte solvents and VC as a functional additive (co-solvent). The composition of the formulation was altered in a systematic way by varying the concentration of only one component and keeping all remaining components constant. The $LiPF_6$ concentration was allowed to vary between 0.2 mol/kg and 2.3 mol/kg. The ratio of EC/EMC solvent mixture was varied from 0.43 to 3.0 by weight. The concentration of VC was varied between 0 and 30 wt% with respect to the solvents. In total, 56 electrolytes were fully automatically formulated by means of the HTE system positioned in the glovebox (MBraun, H_2O and $O_2 <$ 1 ppm) under N_2 atmosphere, of which 48 could be used for conductivity determination. In the other cases, crystal formation was either directly observed or deducted from recorded conductivity data. For exact compositions of all considered electrolyte formulations see the Supporting Information.

Conductivity determination

All experiments were carried out under an inert atmosphere (Ar or N_2). Conductivity cells were filled and sealed via HTE system in the glovebox (MBraun, H_2O and $O_2 < 1$ ppm). Cell constants were determined with a 0.01 M solution of KCl at 20 °C (VWR, known conductivity of 1.276 mS cm^{1}) and averaged over five measurements. Disposable 2 mL Eppendorf Safe-Lock Tubes were used as sample containers and filled with 750 µL of electrolyte each. Impedance measurements were conducted on a Metrohm Autolab/M204 potentiostat/galvanostat with 12 channels and 8-channel multiplexer for a total of 96 channels in the range of 50 Hz to 20000 Hz using in-house developed electrodes.[34] The samples were placed in a temperature chamber (Memmert TTC256, 0.1 °C temperature setting accuracy) and each temperature was held for 2 h prior to measurement for equilibration. Obtained impedance spectra were fitted using a model specified with set parameters for resistors R_s and R_p, as well as for the constant phase element (CPE) with the Metrohm Nova software. The fitting model R1 + R2/Q was used as standard. Due to the use of ion-blocking electrodes, R2 can be approximated to infinite and the model simplifies to R1 + Q, which only contains the essential resistance R1 for the automated observation of the total ionic conductivity of the considered electrolyte formulations. The fit was carried out after each additional measuring point.

Data-driven analysis

All data are extracted from HT experiments with conducting salt ($LiPF_6$), solvent (EC), additive (VC) compositions (X = (x1,x2,x3)) and temperature (T) as features and ionic conductivity as target quantity. For details on applied surrogate models and GPR results see the Supporting Information.

Acknowledgements

This project has received funding from the European Union's Horizon 2020 research and innovation programme under grant agreement No 957189. The high-throughput experimentation facility was developed in-house within the project Elektrolytlabor 4^E (project grant number: 03X4632). We acknowledge helpful discussions with Prof. X. Jiang.

Conflict of Interest

The authors declare no conflict of interest.

Data Availability Statement

The data that support the findings of this study are openly available in ChemRxiv at https://doi.org/10.26434/chemrxiv-2022-vbl5d, reference number 2022.

Keywords: High-throughput screening · Data driven analysis · Machine learning · Liquid electrolyte · Ionic conductivity

[1] S. M. Mennen, C. Alhambra, C. L. Allen, M. Barberis, S. Berritt, T. A. Brandt, A. D. Campbell, J. Castañón, A. H. Cherney, M. Christensen, D. B. Damon, J. Eugenio de Diego, S. García-Cerrada, P. García-Losada, R. Haro, J. Janey, D. C. Leitch, L. Li, F. Liu, P. C. Lobben, D. W. C. MacMillan, J. Magano, E. McInturff, S. Monfette, R. J. Post, D. Schultz, B. J. Sitter, J. M. Stevens, I. I. Strambeanu, J. Twilton, K. Wang, M. A. Zajac, *Org. Process Res. Dev.* **2019**, *23*, 1213–1242.
[2] R. Potyrailo, K. Rajan, K. Stoewe, I. Takeuchi, B. Chisholm, H. Lam, *ACS Comb. Sci.* **2011**, *13*, 579–633.
[3] B. Burger, P. M. Maffettone, V. V. Gusev, C. M. Aitchison, Y. Bai, X. Wang, X. Li, B. M. Alston, B. Li, R. Clowes, N. Rankin, B. Harris, R. S. Sprick, A. I. Cooper, *Nature* **2020**, *583*, 237–241.
[4] M. Shevlin, *ACS Med. Chem. Lett.* **2017**, *8*, 601–607.
[5] M. Benz, A. Asperger, M. Hamester, A. Welle, S. Heissler, P. A. Levkin, *Nat. Commun.* **2020**, *11*, 5391.
[6] P. Szymański, M. Markowicz, E. Mikiciuk-Olasik, *Int. J. Mol. Sci.* **2011**, *13*, 427–452.
[7] J. R. Hattrick-Simpers, J. M. Gregoire, A. G. Kusne, *APL Mater.* **2016**, *4*, 053211.
[8] N. Blow, *Nat. Methods* **2009**, *6*, 105–108.
[9] S. Chakraboty, W. Xie, N. Mathews, M. Sherburne, R. Ahuja, M. Asta, S. G. Mhaisalkar, *ACS Energy Lett.* **2017**, *2*, 837–845.
[10] B. P. MacLeod, F. G. L. Parlane, T. D. Morrissey, F. Häse, L. M. Roch, K. E. Dettelbach, R. Moreira, L. P. E. Yunker, M. B. Rooney, J. R. Deeth, V. Lai, G. J. Ng, H. Situ, R. H. Zhang, M. S. Elliott, T. H. Haley, D. J. Dvorak, A. Aspuru-Guzik, J. E. Hein, C. P. Berlinguette, *Sci. Adv.* **2020**, *6*, eaaz8867.
[11] J. G. de Vries, L. Lefort, *Oil Gas Sci. Technol.* **2013**, *68*, 519–528.
[12] R. Hahn, M. Ferch, K. Tribowski, N. A. Kyerematen, K. Hoeppner, K. Marquardt, K.-D. Lang, W. Bock, *Microsyst. Technol.* **2019**, *25*, 1137–1149.
[13] A. Dave, J. Mitchell, S. Burke, H. Lin, J. Whitacre, V. Viswanathan, **2021**, arXiv preprint DOI 10.48550/ARXIV.2111.14786.
[14] L. Cheng, R. S. Assary, X. Qu, A. Jain, S. P. Ong, N. N. Rajput, K. Persson, L. A. Curtiss, *J. Phys. Chem. Lett.* **2015**, *6*, 283–291.
[15] C. Lv, X. Zhou, L. Zhong, C. Yan, M. Srinivasan, Z. W. Seh, C. Liu, H. Pan, S. Li, Y. Wen, Q. Yan, *Adv. Mater.* **2021**, 2101474.

[16] S. DiLuzio, V. Mdluli, T. U. Connel, J. Lewis, V. VanBenschoten, S. Bernhard, *J. Am. Chem. Soc.* **2021**, *143*, 1179–1194.
[17] J. Schmidt, M. R. G. Marques, S. Botti, M. A. L. Marques, *Npj Comput. Mater.* **2019**, *5*, 83.
[18] Y. Li, K. Liu, A. M. Foley, A. Zulke, M. Berecibar, E. Nanini Maury, M. Joeri Van, H. E. Hoster, *Renewable Sustainable Energy Rev.* **2019**, *113*, 109254.
[19] R. Eslamloueyan, M. H. Khademi, S. Mazinani, *Ind. Eng. Chem. Res.* **2011**, *50*, 4050–4056.
[20] G. Sivaraman, A. N. Krishnamoorthy, M. Baur, C. Holm, M. Stan, G. Csányi, C. Benmore, Á. Vázquez-Mayagoitia, *Npj Comput. Mater.* **2020**, *6*, 1–8.
[21] G. Sivaraman, L. Gallington, A. N. Krishnamoorthy, M. Stan, G. Csányi, Á. Vázquez-Mayagoitia, C. J. Benmore, *Phys. Rev. Lett.* **2021**, *126*, 156002.
[22] A. Dave, J. Mitchell, K. Kandasamy, H. Wang, S. Burke, B. Paria, B. Póczos, J. Whitacre, V. Viswanathan, *Cell Rep.* **2020**, *1*, 100264.
[23] S. K. Saikin, C. Kreisbeck, D. Sheberla, J. S. Becker, A. Aspuru-Guzik, *Expert Opin. Drug Discovery* **2019**, *14*, 1–4.
[24] A. Benayad, D. Diddens, A. Heuer, A. N. Krishnamoorthy, M. Maiti, F. L. Cras, M. Legallais, F. Rahmanian, Y. Shin, H. Stein, M. Winter, C. Wölke, P. Yan, I. Cekic-Laskovic, *Adv. Energy Mater.* **2021**, 2102678.
[25] T. Lombardo, M. Duquesnoy, H. El-Bouysidy, F. Årén, A. Gallo-Bueno, P. B. Jørgensen, A. Bhowmik, A. Demortière, E. Ayerbe, F. Alcaide, M. Reynaud, J. Carrasco, A. Grimaud, C. Zhang, T. Vegge, P. Johansson, A. A. Franco, *Chem. Rev.* **2021**, https://doi.org/10.1021/acs.chemrev.1c00108.
[26] A. V. Karatrantos, M. S. Khan, C. Yan, R. Dieden, K. Urita, T. Ohba, Q. Cai, *J. Energy Power Technol. - LiDSEN* **2021**, *3*, DOI 10.21926/jept.2103043.
[27] M. Winter, B. Barnett, K. Xu, *Chem. Rev.* **2018**, *118*, 11433–11456.
[28] K. Xu, *Chem. Rev.* **2004**, *104*, 4303–4418.
[29] O. Borodin, G. D. Smith, *J. Phys. Chem. B* **2009**, *113*, 1763–1776.
[30] K. Oldiges, D. Diddens, M. Ebrahiminia, J. B. Hooper, I. Cekic-Laskovic, A. Heuer, D. Bedrov, M. Winter, G. Brunklaus, *Phys. Chem. Chem. Phys.* **2018**, *20*, 16579–16591.
[31] O. Borodin, M. Olguin, P. Ganesh, P. R. C. Kent, J. L. Allen, W. A. Henderson, *Phys. Chem. Chem. Phys.* **2016**, *18*, 164–175.
[32] T. M. Ong, O. Verners, E. Draeger, W. A. van Duin, C. T. V. Lordi, J. E. Pask, *J. Phys. Chem. B* **2015**, *119*, 1535–1545.
[33] I. Cekic-Laskovic, N. von Aspern, L. Imholt, S. Kaymaksiz, K. Oldiges, B. R. Rad, M. Winter, *Top. Curr. Chem.* **2017**, *375*, 37.
[34] H.-D. Wiemhöfer, M. Grünebaum, M. M. Hiller, *MICRO ELECTRODE LIQUID MEASUREMENT CELL*, **2014**, WO 2014/139494 A1.
[35] P. Y. Zavalij, S. Yang, M. S. Wittingham, **2005**, DOI 10.5517/cc86mdg.
[36] M. S. Ding, K. Xu, S. Zhang, K. Amine, G. L. Henriksen, R. Jow, *J. Electrochem. Soc.* **2001**, *148*, A1196–1204.
[37] J. Landesfeind, H. A. Gasteiger, *J. Electrochem. Soc.* **2019**, *166*, A3079–A3097.
[38] C. E. Rasmussen, C. K. I. Williams, *Gaussian Processes for Machine Learning*, MIT Press, Cambridge, Mass, **2006**.
[39] D. K. Duvenaud, *Automatic Model Construction with Gaussian Processes*, University of Cambridge, **2014**.
[40] I. Fomenko, M. Durst, D. Balaban, *Comput. Methods Programs Biomed.* **2006**, *82*, 31–37.
[41] D. Eck, *Stat. Probab. Lett.* **2017**, *134*, DOI 10.1016/j.spl.2017.11.001.
[42] J. Fox, "Bootstrapping Regression Models," can be found under https://artowen.su.domains/courses/305-1314/FoxOnBootingRegInR.pdf, **2002**.
[43] E. R. Logan, E. M. Tonita, K. L. Gering, J. Li, X. Ma, L. Y. Beaulieu, J. R. Dahn, *J. Electrochem. Soc.* **2018**, *165*, A21–A30.
[44] S. Solchenbach, M. Metzger, M. Egawa, H. Beyer, H. A. Gasteiger, *J. Electrochem. Soc.* **2018**, *165*, A3022–A3028.
[45] H. P. Chen, J. W. Fergus, B. Z. Jang, *J. Electrochem. Soc.* **2000**, *142*, 399–406.
[46] A. N. Krishnamoorthy, K. Oldiges, M. Winter, A. Heuer, I. Cekic-Laskovic, C. Holm, J. Smiatek, *Phys. Chem. Chem. Phys.* **2018**, *20*, 25701–25715.
[47] K. Xu, Y. Lam, S. S. Zhang, T. R. Jow, T. B. Curtis, *J. Phys. Chem. C* **2007**, *111*, 7411–7421.
[48] L. O. Valøen, J. N. Reimers, *J. Electrochem. Soc.* **2005**, *152*, A882.
[49] A. Nyman, M. Behm, G. Lindbergh, *Electrochim. Acta* **2008**, *53*, 6356–6365.
[50] D. Aurbach, K. Gamolsky, B. Markovsky, Y. Gofer, M. Schmidt, U. Heider, *Electrochim. Acta* **2002**, *47*, 1423–1439.
[51] Y. Qian, C. Schultz, P. Niehoff, T. Schwieters, S. Nowak, F. M. Schappacher, M. Winter, *J. Power Sources* **2016**, *332*, 60–71.
[52] M.-M. Walz, D. van der Spoel, *Commun. Chem.* **2021**, *4*, 9.
[53] V. Makarenkov, D. Kevorkov, P. Zentilli, A. Gagarin, N. Malo, R. Nadon, *Bioinformatics* **2006**, *22*, 1408–1409.
[54] J. Rein, J. R. Annand, M. K. Wismer, J. Fu, J. C. Siu, A. Klapars, N. A. Strotman, D. Kalyani, D. Lehnherr, S. Lin, *ACS Cent. Sci.* **2021**, *7*, 1347–1355.
[55] S. Matsuda, K. Nishioka, S. Nakanishi, *Sci. Rep.* **2019**, *9*, 6211.

Manuscript received: February 12, 2022
Version of record online: June 10, 2022